Chinese Journal of
POLYMER SCIENCE

RESEARCH ARTICLE

https://doi.org/10.1007/s10118-025-3412-9
Chinese J. Polym. Sci. **2025**, *43*, 2128–2137

Atif-V2.0: Extending Classical Density Functional Theory with Interfacial Statistical Associating Fluid Theory for Inhomogeneous Associating Fluids

Xiu-Jun Wang[a,b], Shi-Chao Li[a,b], Jian Zhang[a,b], Qiu-Hui Chang[c*], and Jian Jiang[c,d*]

[a] *CNOOC Research Institute Co., Ltd., Beijing 100028, China*
[b] *State Key Laboratory of Offshore Oil and Gas Exploitation, Beijing 102209, China*
[c] *Beijing National Laboratory for Molecular Sciences, State Key Laboratory of Polymer Physics and Chemistry, Institute of Chemistry, Chinese Academy of Sciences, Beijing 100190, China*
[d] *University of Chinese Academy of Sciences, Beijing 100049, China*

Electronic Supplementary Information

Abstract Understanding the thermodynamic behavior of complex fluids in confined environments is critical for various industrial and natural processes including but not limited to polymer flooding enhanced oil recovery (EOR). In this work, we develop Atif-V2.0, an extended classical density functional theory (cDFT) framework that integrates the interfacial statistical associating fluid theory (iSAFT) to model multicomponent associating fluids composed of water-soluble polymers, alkanes, and water. Building on the original theoretical framework of Atif for modeling nanoconfined inhomogeneous fluids, Atif-V2.0 embeds explicit solvent and captures additional physical interactions - hydrogen bonding, which are critical in associating fluid systems. The other key feature of Atif-V2.0 is its ability to account for polymer topology. We demonstrate its capability by predicting the equilibrium structure and thermodynamic behavior of branched hydrolyzed polyacrylamide solutions near hard walls with various branching topologies, which provides a robust theoretical tool for the rational design of EOR polymers.

Keywords Classical density functional theory; Interfacial statistical associating fluid theory; Hydrogen bonding; Associating fluid

Citation: Wang, X. J.; Li, S. C.; Zhang, J.; Chang, Q. H.; Jiang, J. Atif-V2.0: extending classical density functional theory with interfacial statistical associating fluid theory for inhomogeneous associating fluids. *Chinese J. Polym. Sci.* **2025**, *43*, 2128–2137.

INTRODUCTION

With the continuous growth in global energy demand and the gradual depletion of conventional oil reservoirs, enhancing oil recovery (EOR) has become a crucial challenge in the petroleum industry.[1–3] In complex reservoir conditions characterized by high water content, salinity, temperature, and pressure, the efficacy of conventional water flooding has declined significantly. This necessitates the advancement of more efficient and controllable chemical flooding methodologies. Among them, polymer flooding is one of the most established and widely used techniques.[4–6] It works by injecting water-soluble polymers to enhance the viscosity of the displacing fluid, thereby improving its mobility and oil recovery.

Hydrolyzed polyacrylamide (HPAM) is the most commonly used polymer in EOR [7,8] due to its exceptional viscosifying ability, which is attributed to its high molecular weight and presence of charges. However, linear HPAM faces several limitations under harsh reservoir conditions.[9–13] In high-salinity environments, its viscosity decreases markedly due to the contraction of molecular chains caused by the reduced ionic repulsion.[14–17] Moreover, its long, flexible chains are prone to degradation under high shear rates and temperatures.[18,19] To overcome these challenges, various studies have focused on modifying HPAM chain architectures, including star, branched, and hyperbranched structures.[20–29] It has been shown that introducing branched chains with hydrophobic side groups can enhance shear resistance, as well as tolerance to salinity and temperature.[21] Despite these advances, the vast design space of tunable polymer structures makes experiments and computationally intensive molecular simulations (including those accelerated by emerging machine learning force fields[30,31]) inefficient in the pursuit of water-soluble polymers with optimal properties for the demanding conditions of EOR. This limitation becomes more pronounced when seeking optimal chain architectures across a wide range of salinity, temperature, and confinement conditions, which strongly affect polymer performance in subsurface environments.

To gain deeper insight into the effect of chain structures on

* Corresponding authors, E-mail: cqiuhui@iccas.ac.cn (Q.H.C.)
E-mail: jiangj@iccas.ac.cn (J.J.)

Received June 6, 2025; Accepted July 7, 2025; Published online September 24, 2025

the thermodynamic behavior of branched HPAM (BHPAM) under realistic reservoir conditions, theoretical approaches that combine molecular-level resolution with computational efficiency are essential. Classical density functional theory (cDFT), grounded in statistical mechanics, has proven to be an effective tool for modeling equilibrium structures and thermodynamic properties of inhomogeneous complex fluids.[32–36] We have developed a cDFT-based software, Atif (Advanced Theoretical Tool for Inhomogeneous Fluids),[37] which incorporates key interactions such as hard-sphere repulsion, mean-field electrostatics, and electrostatic correlations. This theory has been successfully applied to systems such as polyelectrolyte solutions and polycation - polyanion mixtures.[38–40] However, its predictive capability remains limited for multicomponent associative fluids such as complex mixtures containing BHPAM, oil, and water, where hydrogen bonding between BHPAM and water plays a critical role.

Statistical associating fluid theory (SAFT)[41–43] and its variants such as Perturbed - Chain SAFT (PC-SAFT),[44] for potential of variable range (SAFT-VR),[45] interfacial SAFT (iSAFT),[46,47] and SAFT-γ Mie[48] provide a promising solution to the limitations of Atif software. Several studies have demonstrated that constructing Helmholtz free energy functionals by integrating SAFT or its variants with cDFT enables accurate predictions of polymer or alkane density profiles in confined media.[49–53] These hybrid models have demonstrated good agreement with molecular simulations, validating their applicability to inhomogeneous associating fluids at solid–liquid interfaces. However, most existing studies have overlooked the role of polymer topology. To the best of our knowledge, there are only work from Tripathi and Chapman using iSAFT-DFT to investigate the microstructure and thermodynamic properties of branched polymer blends or solutions near a hard surface.[47,52] Notably, their approach employed an implicit solvent model, which cannot account for hydrogen bonding between water and polymers. More recently, Chapman and co-workers developed a new iSAFT framework incorporating an explicit solvent model to study micelle formation and interfacial properties of surfactants.[46] This advancement demonstrates the capability of iSAFT-based theories to capture hydrogen-bonding interactions. However, the simultaneous incorporation of confinement effects, polymer branching topology, and explicit hydrogen bonding within a unified theoretical framework remains unexplored.

To address these outstanding challenges and enable accurate modeling of polymer flooding in realistic porous environments, we developed Atif-V2.0 by introducing two major enhancements. First, the bonding potential was modified to enable the treatment of arbitrary chain topologies of polymer. In addition, an associative attraction term was added to the excess Helmholtz free energy to explicitly account for hydrogen bonding, following the iSAFT framework proposed by Chapman.[46] These improvements collectively allow Atif-V2.0 to describe both polymer topology and associative interactions in confined aqueous environments. The goal of this work is to demonstrate the feasibility of using iSAFT-cDFT to predict the equilibrium structures and thermodynamic properties of water-soluble polymer solutions with various branching topologies under nanoconfinement.

MODEL AND THEORY

In polymer flooding for EOR, water-soluble polymers such as BHPAM are injected into porous reservoir rocks to improve oil displacement efficiency. After the initial water flooding stage, the remaining pore space typically contains minimal crude oil, and the injected polymer solution primarily consists of BHPAM and water. As illustrated in Fig. 1(a), the polymer solution flows through confined geometries resembling interconnected slit-like pores. Within these confined aqueous environments, the BHPAM chains experience complex interactions with water, oils,

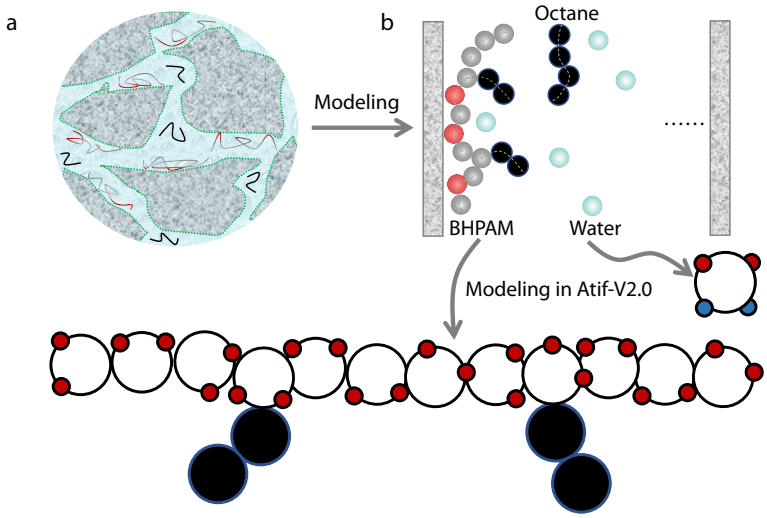

Fig. 1 (a) A conceptual representation of the polymer flooding system, where polymer, oil, and water are stored within the nanoporous structure of reservoir rocks. (b) Schematic illustration of the modeling framework for polymer/oil/water mixtures. Oils are represented by hydrophobic hard-sphere chains, with octane serving as a representative species. Water molecules are modeled using a four sites model: two electron donor (A^+) and two electron acceptor sites (B^-)). Branched HPAM is modeled as a hard-sphere chain where the carboxylate groups are modeled as segments with two electron acceptor sites (C^-) and the groups in the side chains are modeled as segments with alkane-like parameters.

https://doi.org/10.1007/s10118-025-3412-9

and pore walls. To gain fundamental insight into the polymer's thermodynamic behavior under such conditions, we consider a simplified model system comprising BHPAM, oil, and water confined between two parallel plates. This reductionist approach captures the essential physics governing polymer distribution and conformation in EOR- relevant environments.

To analyze these systems from a molecular thermodynamic perspective, we employ iSAFT-cDFT software package named Atif-V2.0 (an advanced theoretical tool for inhomogeneous fluids,[37] Version 2.0), which is adept at handling multicomponent associative fluids containing linear or branched polymers, alkanes, and water. To simplify the demonstration, we focus on a representative system within EOR scenario, which comprises of BHPAM, octane, and water. The molecular models of this system are illustrated in Fig. 1(b). In realistic reservoir conditions, partial hydrolysis of the polyacrylamide backbone converts some acrylamide groups into carboxylate groups, which can participate in both hydrogen bonding and electrostatic interactions. However, to isolate and systematically consider the role of hydrogen bonding between BHPAM and water, electrostatic interactions are omitted in this work. Accordingly, the BHPAM backbone is modeled as a sequence of segments, each carrying two electron acceptor sites, representing the hydrogen bond acceptor capabilities of acrylamide or hydrolyzed carboxylate groups. The hydrophobic side chains are modeled as alkane-like segments without association sites. In addition, water is modeled as a spherical molecule with four association sites, consisting of two electron donor and two electron acceptor sites. Octane is represented as a chain of four alkane-like monomers without any association sites.

By following the framework of density functional theory (DFT), the analytical expression of the grand potential for systems with BHPAM and water/oil mixtures can be written as

$$W = \mathcal{F}_{\mathrm{id}} + \mathcal{F}_{\mathrm{ex}} + \sum_p \int \mathrm{d}\mathbf{R}\rho_{\mathrm{p}}(\mathbf{R})\left[\psi_{\mathrm{p}}(\mathbf{R}) - \mu_{\mathrm{p}}\right] + \sum_\alpha \int \mathrm{d}\mathbf{r}\rho_\alpha(\mathbf{r})\left[\psi_\alpha(\mathbf{r}) - \mu_\alpha\right] \tag{1}$$

where $p \in \{\mathrm{Hp}, \mathrm{Oc}\}$. Here, Hp and Oc refer to BHPAM and Octane, respectively. In Eq. (1), $\mathrm{d}\mathbf{R} = \mathrm{d}\mathbf{r}_1\mathrm{d}\mathbf{r}_2\cdots\mathrm{d}\mathbf{r}_N$ with $N_{\mathrm{Oc}} = 4$ and $N_{\mathrm{Hp}} = n_x + bn_y$, where b is the number of side chains. $\rho_{\mathrm{p}}(\mathbf{R})$ is the $3N$ -dimensional segments density distribution of the BHPAM chains or Octanes. $\mathbf{r}$ is the 3-dimensional coordinates of the particles. μ_{P} is the chemical potentials of BHPAM or Octane, and μ_α is the chemical potentials of water. The non-electrostatic external potential $\Psi_{\mathrm{p}}(\mathbf{R})$ is applied to the entire chain of BHPAM or Octane. *i.e.*, $\Psi_{\mathrm{p}}(\mathbf{R}) = \sum_{m=1}^{N_{\mathrm{Hp}}}\psi_{\mathrm{p},m}(\mathbf{r}_{\mathrm{p},m})$, where m is the index of segment and $\psi_{\mathrm{p},m}(\mathbf{r})$ is the external potential imposed on the individual segments. In this work, the non-electrostatic external potential is modeled as a normalized and truncated 9-3 Lennard-Jones (LJ 93) wall potential

$$\beta\psi_i(r) = \begin{cases} +\infty & r < R_i \text{ or } r > h - R_i \\ \beta u_i(z) & R_i \le r \le z_{\mathrm{c}} \text{ or } h - z_{\mathrm{c}} \le r \le h - R_i \\ 0 & \text{otherwise} \end{cases} \tag{2}$$

with

$$\beta u_i(z) = \epsilon_i \frac{1}{u_i^*(z_{\mathrm{m}}) - u_i^*(z_{\mathrm{c}})}\left[u_i^*(z - R_i + z_{\mathrm{m}}) - u_i^*(z_{\mathrm{c}})\right] \tag{3}$$

where ϵ_i is the depth of the potential well. $\epsilon_i > 0$ and $\epsilon_i < 0$ refer to the purely repulsive and attractive wall-particle interactions, respectively. R_i is the radius of segment i ($R_i = \sigma_i/2$). $u^*(z)$ denotes the standard LJ 9-3 potential between a spherical particle and a planar surface, given by

$$u_i^*(z) = \epsilon_i^*\left[\frac{2}{15}\left(\frac{\sigma_i}{z}\right)^9 - \left(\frac{\sigma_i}{z}\right)^3\right] \tag{4}$$

where σ_i is the diameter of segments. In Eq. (3), $z_{\mathrm{c}} = \gamma_{\mathrm{c}}\sigma_i$ is the cutoff distance at which the external potential $u_i^*(z)$ is set to zero (with $\gamma_{\mathrm{c}} = 1.2$), and z_{m} is the distance where $u_i^*(z)$ reaches its minimum.

The ideal free energy $\mathcal{F}_{\mathrm{id}}$ in Eq. (1) is given by

$$\beta\mathcal{F}_{\mathrm{id}} = \sum_p \int \mathrm{d}\mathbf{R}\rho_{\mathrm{p}}(\mathbf{R})\left\{\ln\left[\rho_{\mathrm{p}}(\mathbf{R})a^N\right] - 1\right\} + \sum_p \int \mathrm{d}\mathbf{R}\rho_{\mathrm{p}}(\mathbf{R})\beta V_{\mathrm{b,p}}(\mathbf{R}) + \sum_\alpha \int \mathrm{d}\mathbf{r}\rho_\alpha(\mathbf{r})\left\{\ln\left[\rho_\alpha(\mathbf{r})a\right] - 1\right\} \tag{5}$$

where $p \in \{\mathrm{Hp}, \mathrm{Oc}\}$. In above equation, a can be taken as the cube of the thermal de Broglie length which is immaterial as it has no thermodynamic consequences. The total monomer density of Octane $\rho_{\mathrm{Oc}}(\mathbf{r})$ is related to $\rho_{\mathrm{Oc}}(\mathbf{R})$ *via*

$$\rho_{\mathrm{Oc}}(\mathbf{r}) = \sum_{k=1}^{N_{\mathrm{Oc}}}\int \mathrm{d}\mathbf{R}\delta\left(\mathbf{r} - \mathbf{r}_{\mathrm{Oc}}^k\right)\rho_{\mathrm{Oc}}(\mathbf{R}) \tag{6}$$

Analogously, the total monomer density of m^{th} part of BHPAM $\rho_{\mathrm{Hp}}^m(\mathbf{r})$ is related to $\rho_{\mathrm{Hp}}(\mathbf{R})$ *via*

$$\rho_{\mathrm{Hp}}^m(\mathbf{r}) = \sum_{k=1}^{n_m}\int \mathrm{d}\mathbf{R}\delta\left(\mathbf{r} - \mathbf{r}_{\mathrm{Hp},m}^k\right)\rho_{\mathrm{Hp}}(\mathbf{R}) \tag{7}$$

where $m \in \{x, y\}$, x and y refer to the backbone and branch chain of BHPAM, respectively.

In this work, the bonding potential $V_{\mathrm{b,Oc}}(\mathbf{R})$ of Octane chain is defined as

$$\exp\left[-\beta V_{\mathrm{b,Oc}}(\mathbf{R})\right] = a^{N_{\mathrm{Oc}}-1}\prod_{i=2}^{N_{\mathrm{Oc}}}\frac{\delta\left(\left|\mathbf{r}_{\mathrm{Oc}}^{i-1} - \mathbf{r}_{\mathrm{Oc}}^i\right| - \sigma\right)}{4\pi\sigma^2} \tag{8}$$

where $N_{\mathrm{Oc}} = 4$. The bonding potential $V_{\mathrm{b,Hp}}(\mathbf{R})$ of BHPAM chain is

$$\exp\left[-\beta V_{\mathrm{b,Hp}}(\mathbf{R})\right] = a^{N_{\mathrm{Hp}}-1}\prod_{i=2}^{n_x+n_y}\frac{\delta\left(\left|\mathbf{r}_{\mathrm{Hp}}^{i-1} - \mathbf{r}_{\mathrm{Hp}}^i\right| - \sigma\right)}{4\pi\sigma^2} \times \prod_{j=1}^{b}\prod_{k=1}^{n_z}\frac{\delta\left(\left|\mathbf{r}_{\mathrm{Hp}}^{j,k-1} - \mathbf{r}_{\mathrm{Hp}}^{j,k}\right| - \sigma\right)}{4\pi\sigma^2} \tag{9}$$

where b is the number of side chains on the BHPAM and $\mathbf{r}_{\mathrm{Hp}}^{j,k}$ is the coordinate of the k^{th} monomer on the j^{th} side chain. We have to note that $\mathbf{r}_{\mathrm{Hp}}^{j,0}$ is the coordinate of monomer on the backbone of BHPAM.

In Eq. (1), the excess Helmholtz free energy $\mathcal{F}_{\mathrm{ex}}$ in Atif-V2.0 is formulated as

$$\mathcal{F}_{\mathrm{ex}} = \mathcal{F}_{\mathrm{hc}} + \mathcal{F}_{\mathrm{assoc}} \tag{10}$$

The original theoretical framework in Atif has implemented the excess Helmholtz free energy derived from the hard-core excluded volume interaction ($\mathcal{F}_{\mathrm{hc}}$). The more details of this legacy term are provided in the electronic supplemen-

tary information (ESI). In Atif-V2.0, the excess Helmholtz free energy also includes the contribution from the associative attraction ($\mathcal{F}_{\text{assoc}}$).

The Helmholtz free energy functional for associative attractions is constructed using WDA as shown in Sauer and Gross' work.[51] In the bulk system, this Helmholtz free energy functional consistent with the association contribution in iSAFT equation of state. The associative Helmholtz free energy functional is

$$\mathcal{F}_{\text{assoc}} = \int \mathrm{d}\mathbf{r} f_{\text{assoc}}\left[\{\rho_i(\mathbf{r})\}\right] \tag{11}$$

with the associative Helmholtz free energy density being

$$\beta f_{\text{assoc}} = \sum_i \frac{n_{0i}}{N_i}\zeta_i \sum_{A_i} M_{A_i}\left(\ln\chi_{A_i}(\mathbf{r}) - \frac{\chi_{A_i}(\mathbf{r})}{2} + \frac{1}{2}\right) \tag{12}$$

where the outer summation runs over all components and the inner summation runs over all types of association sites of species i. M_{A_i} is the number of association sites of type A_i on species i and $\chi_{A_i}(\mathbf{r})$ is locally defined fraction of association sites A_i components i which are not bonded. This fraction is given by

$$\chi_{A_i}(\mathbf{r}) = \left[1 + \sum_j \frac{n_{0j}(\mathbf{r})}{N_j}\zeta_j(\mathbf{r}) \sum_{B_j} M_{B_j}\chi_{B_j}(\mathbf{r})\Delta^{A_iB_j}(\mathbf{r})\right]^{-1} \tag{13}$$

with $\Delta^{A_iB_j}(\mathbf{r})$ as the locally defined association strength between association sites A_i and B_j

$$\Delta^{A_iB_j}(\mathbf{r}, \mathbf{r}') = \sigma_{ij}^3 \kappa^{A_iB_j}\left[\exp\left(\beta\varepsilon^{A_iB_j}\right) - 1\right] g_{ij}^{\text{hs}}\left(d_{ij}; n_\alpha(\mathbf{r})\right) \tag{14}$$

where B_j represents the segments which can associate with segments A_i, this association can be used to explain the hydrogen bonding to a degree. The hydrogen bonding interaction energy is model by an orientationally dependent square well potential

$$u_{AB}^{\text{assoc}}(r, \Omega_i, \Omega_j) = \begin{cases} -\varepsilon^{A_iB_j} & r < r_c^{\text{assoc}}; \theta_A < \theta_c; \theta_B < \theta_c \\ 0 & \text{otherwise} \end{cases} \tag{15}$$

where $\epsilon^{A_iB_j}$ is the association energy strength. r_c^{assoc} is the cutoff distance within which association can occur. Ω_i and Ω_j are the orientations of segments i and j. θ is the angle between the vector pointing from the center of a segment to the center of the association site on that segment and the vector pointing from the center of one segment (i or j) to the center of the other segment (i or j). Association can only occur when these two angles (θ_A and θ_B) are smaller than the cutoff value θ_c. The cutoff distance and the angular cutoffs are chosen to allow only one bond per association site. In Eq. (14), $\kappa^{A_iB_j}$ is a bonding geometric constant. The association parameters used for each component are suggested by Chapman[46] and shown in Table 1, which were optimized within the iSAFT framework to reproduce experimental measurements of pure component liquid densities and vapor pressures.

The radial distribution function of hard-spheres g_{ij}^{hs} at contact is given as

$$g_{ij}^{\text{hs}}\left(d_{ij}; \{n_\alpha(\mathbf{r})\}\right) = \frac{1}{1-n_3} + \frac{d_i d_j}{d_{ij}}\frac{n_2\zeta}{4(1-n_3)^2} + \left(\frac{d_i d_j}{d_{ij}}\right)^2 \frac{n_2^2\zeta}{72(1-n_3)^3} \tag{16}$$

where $d_{ij} = \left(d_i + d_j\right)/2$. In Eqs. (12)–(16), the weighted densities

Table 1 Summary of parameters. In this table, the alkane-like monomer is used to model the hydrophobic groups on the backbone and side chains of HPAM.

	N_i	$\epsilon_{\text{assoc}}/k_{\text{B}}$(K)	κ/σ_i^3
Water (i = 1)[46]	1	1747.3	0.004432
Octane (i = 2)[46]	4	0	0
Backbone of BHPAM (i = 3)	$n_x^{(1)}$	1747.3	0.004432
Branch chain of BHPAM (i = 4)	$n_y^{(2)}$	0	0

(1) the number of acrylamide monomers on the backbone of BHPAM; (2) the number of alkane-like monomers on the branch chain of BHPAM.

$\{n_{ai}\}$ and $\{n_a\}$ as well as the correction factors ζ_i and ζ are defined according to Yu and Wu[54]

$$n_\alpha = \sum_i n_{ai} = \int d\mathbf{r}' \rho_i(\mathbf{r}') w_i^{(\alpha)}(\mathbf{r}-\mathbf{r}'),\ \alpha = \{0, 1, 2, 3, V_1, V_2\} \tag{17}$$

$$\zeta_i = 1 - \frac{\mathbf{n}_{V_2 i}\mathbf{n}_{V_2 i}}{n_{2i}^2} \tag{18}$$

$$\zeta = 1 - \frac{\mathbf{n}_{V_2}\mathbf{n}_{V_2}}{n_2^2} \tag{19}$$

In the above equations, the weighted functions $\left\{w_i^{(\alpha)}(\mathbf{r})\right\}$ are defined by the FMT: $w_i^{(3)}(\mathbf{r}) = \Theta(d_i/2 - |\mathbf{r}|)$, $w_i^{(2)}(\mathbf{r}) = \delta(d_i/2 - |\mathbf{r}|)$, $w_i^{(1)}(\mathbf{r}) = w_i^{(2)}(\mathbf{r})/2\pi d_i$, $w_i^{(0)}(\mathbf{r}) = w_i^{(2)}(\mathbf{r})/\pi d_i$, $w_i^{(V_2)}(\mathbf{r}) = (\mathbf{r}/r)\,\delta(d_i/2 - |\mathbf{r}|)$, and $w_i^{(V_1)}(\mathbf{r}) = w_i^{(V_2)}(\mathbf{r})/2\pi d_i$.[55]

We rearrange the $\{\chi_{A_i}\} = \{\chi_{\alpha_1}, \chi_{\beta_1}, \chi_{\gamma_1}, \cdots, \chi_{\alpha_2}, \cdots\}$ to $\{\chi_1, \chi_2, \chi_3, \cdots\}$. Then we set $\mathbf{X} = \{\chi_1, \chi_2, \chi_3, \cdots\}$ and $\mathbf{F} = \{f_1 - \chi_1, f_2 - \chi_2, f_3 - \chi_3, \cdots\}$, where

$$f_1 = \left[1 + \sum_j \frac{\rho_j^{\text{b}}}{N_j}\sum_{B_j} M_{B_j}\chi_{B_j}\Delta^{\alpha_1 B_j}\right]^{-1} \tag{20}$$

and

$$f_2 = \left[1 + \sum_j \frac{\rho_j^{\text{b}}}{N_j}\sum_{B_j} M_{B_j}\chi_{B_j}\Delta^{\beta_1 B_j}\right]^{-1} \cdots \tag{21}$$

$$F_i = \left[1 + \sum_j \frac{\rho_j^{\text{b}}}{N_j}\sum_{B_j} M_{B_j}\chi_{B_j}\Delta^{iB_j}\right]^{-1} - \chi_i \tag{22}$$

The Newton step for the set of equations $\mathbf{F} = 0$ is

$$\mathbf{X}_{\text{new}} = \mathbf{X}_{\text{old}} + \delta\mathbf{X}, \tag{23}$$

where

$$\delta\mathbf{X} = -\mathbf{J}^{-1} \times \mathbf{F} \tag{24}$$

with $\mathbf{J} = \{\partial F_i/\partial\chi_j\}$ the Jacobian matrix. We define $f(\mathbf{X}) = \mathbf{F} \times \mathbf{F}/2$. Therefore, the solution of $f = 0$ is also the solution of $\mathbf{F} = 0$. We know that the Newton step of Eq. (24) is a descent direction for f

$$\nabla f \cdot \delta\mathbf{X} = (\mathbf{F} \times \mathbf{J}) \cdot \left(-\mathbf{J}^{-1} \times \mathbf{F}\right) = -F \times F < 0 \tag{25}$$

Therefore, by using the Newton step, the solution of $\mathbf{F} = 0$ is equivalent to the solution of min $\{f\}$. In order to make sure the solution is converged, the new point is updating using

$$\mathbf{X}_{\text{new}} = \mathbf{X}_{\text{old}} + \lambda\delta\mathbf{X},\ 0 < \lambda \le 1 \tag{26}$$

Since the Newton step is the descent direction for f, we first try $\lambda_0 = 1$ (the full Newton step). However, if $f(\mathbf{X}_{\text{new}}) > f(\mathbf{X}_{\text{old}})$, we backtrack along the Newton direction by using $\lambda_{i+1} = \lambda_i/2$.

By minimizing the grand potential with respect to densi-

ties, the equilibrium density profiles of all species can be obtained. Specifically

$$\frac{\delta W}{\delta \rho_{\mathrm{p}}(\mathbf{R})} = 0 \text{ and } \frac{\delta W}{\delta \rho_{\alpha}(\mathbf{r})} = 0 \tag{27}$$

Combining Eqs. (1) and (27) gives

$$\rho_{\mathrm{p}}(\mathbf{R})\, a^{N} = \exp\left\{\beta\left(\mu_{\mathrm{p}} - V_{\mathrm{b,p}}(\mathbf{R}) - \sum_{k=1}^{N} w_{\mathrm{p}}\left(\mathbf{r}_{\mathrm{p}}^{k}\right)\right)\right\} \tag{28}$$

$$\rho_{\alpha}(\mathbf{r})\, a = \exp\{\beta[\mu_{\alpha} - w_{\alpha}(\mathbf{r})]\} \tag{29}$$

where $w_p(\mathbf{r})$ ($p \in \{\mathrm{Hp,Oc}\}$) and $w_\alpha(\mathbf{r})$ refer to the effective fields of BHPAM/octane and water, which can be formulated as $w_j(\mathbf{r}) = \psi_j(\mathbf{r}) + \delta\mathcal{F}_{\mathrm{ex}}/\delta\rho_j(\mathbf{r})$, $j \in [p, \alpha]$. The details of $\delta\mathcal{F}_{\mathrm{assoc}}/\delta\rho_j(\mathbf{r})$ can be found in ESI. Eqs. (28) and (29) can be solved iteratively using a Picard iteration or some other advanced numerical algorithms. The solution flow of Atif- V2.0 is the same as Atif, and the specie details can be found in our previous work.[37]

CASE STUDIES

To illustrate the modeling capabilities of Atif-V2.0 for multicomponent complex associating fluid, we present two application cases that simulate key microscopic behaviors relevant to polymer flooding. The first case focuses on BHPAM/water binary mixtures to examine surface adsorption and distribution behavior of hydrophobic modified BHPAM under nanoconfinement. The second case extends to a more realistic BHPAM/octane/water ternary mixture, aiming to explore how hydrophobic modification influences oil film near solid-liquid interface. In both cases, the polymer concentration is set to 1 mol/L. In addition, the water concentration is set to 20 mol/L, although real aqueous environments typically have water concentrations exceeding 50 mol/L. This simplification is motivated by both physical and numerical considerations. At a high concentration of water, the contribution of excluded volume interaction from water becomes significant, which in turn causes the repulsive functional in the fundamental measure theory to produce excessively large chemical potential differences between the solid-liquid interface and the bulk phase. Such a steep gradient drives unphysical accumulation of polymers near surfaces, deviating from realistic interfacial behavior. It frequently results in significant density field oscillations or convergence failures during iterative processes. To ensure stable and physically meaningful density profiles, we adopted a reduced water concentration. It should be emphasized that our primary goal is to elucidate the molecular mechanism of polymer–surface interactions, with a specific focus on chain topology architectures and hydrophobic association, rather than to fully reproduce the actual composition of polymer aqueous solutions. The modeling setup and physical insights of each case are detailed below.

Case I: BHPAM Aqueous Solution

During polymer flooding, polymer chains may either adsorb onto the pore surfaces or remain dispersed in the bulk aqueous phase.[56,57] Both distribution modes have significant and distinct effects on oil displacement efficiency. On one hand, the adsorption of polymer onto solid surfaces can modify the rock wettability, promoting a water-wet environment that facilitates oil detachment and mobilization. On the other hand, polymers remaining in the solution contribute to increasing the viscosity of the displacing fluid, thereby improving sweep efficiency and reducing water fingering. Striking a balance between surface adsorption and bulk retention is therefore critical for optimizing polymer performance in EOR applications.

The chain architecture is a determinant factor for the behavior of polymer solutions. To elucidate how the topology of polymer chains governs their spatial distribution under confinement, we considered a coarse-grained model of BHPAM aqueous solutions near hard walls. The BHPAM chain is modeled as a flexible backbone with hydrophobic side chains grafted in various patterns. Four different branching architectures, designated as BHPAM-A, -B, -C, and -D, are illustrated in Fig. 2. These chains differ in the length of side chains, the number of branches, and the precise locations of the grafting sites along the backbone. Each backbone segment contains two acceptor sites of hydrogen bonding, enabling specific association with water. The side chains are modeled as tangentially connected hydrophobic groups that interact attractively with the hard walls *via* a LJ-93 wall potential. Since the polymer-surface interaction is highly sensitive to environmental conditions, we systematically investigated three types of attraction strengths ($\epsilon_i = 0, -0.2, -0.4 k_{\mathrm{B}}T$), corresponding to non-attractive, weakly attractive, and strongly attractive conditions.

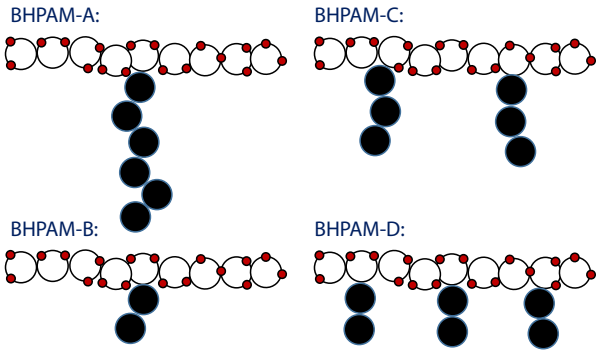

Fig. 2 Schematic diagram illustrating the structure of the hydrophobic-modified BHPAM chain. The chain backbone consists of coarse-grained beads that can form hydrogen bonds with water molecules, where two small red round beads indicate two hydrogen bond binding sites. The black coarse-grained beads on the side chains represent the hydrophobic alkane-like segments.

The competition between conformation entropy penalty and surface attraction plays a dominant role in adsorption behavior of polymers.[58,59] When a chain approaches the surface, its accessible space is significantly restricted, leading to a loss of conformation entropy. This entropic penalty drives the polymer to preferentially adopt conformations away from the surfaces. As a result, polymer chain typically exhibits depletion behavior, as indicated by the normalized density profile below 1 ($\rho(z)/\rho_{\mathrm{b}} < 1$, where ρ_{b} is the density of polymer in bulk). The chains can only enrich near surfaces and form a well-defined adsorbed layer ($\rho(z)/\rho_{\mathrm{b}} > 1$) when the strength of surface attraction adequately compensates for the loss of conformation entropy. Computational results from Atif-V2.0 reveal that the adsorption behavior of BHPAM is primarily governed by the entropic penalty under the non-attractive and weakly attractive conditions. In such cases, the ability of chain topology to modulate conformation entropy becomes

the key factor influencing the density profile of polymers. Notably, at the fixed monomer concentration, polymers with smaller molecular weight (*e.g.*, BHPAM-B) experience lower entropic penalty, making it more favorable for themselves to distribute near surfaces. As shown in Fig. 3(a), the density profiles of BHPAM-B exhibit the lowest degree of depletion among all polymers examined in this work. This advantage diminishes as surface attraction strengthens. The density profiles of BHPAM at different topologies are similar at moderate surface attraction (see Fig. S2 in ESI).

When the attraction between surface and hydrophobic side chains reaches a sufficiently high level (*e.g.*, $\epsilon_i = -0.4k_BT$), the hydrophobic interaction becomes strong enough to overcome the entropic penalty, which allows chain segments to accumulate near surfaces. As shown in Fig. 3(b), the adsorption layers are formed. In this regime, the density differences arising from polymer topology are significantly amplified. BHPAM with a greater number of side chains shows a higher density peak, which means the more stable adsorbed layers and the more excellent adsorption capacity of polymer. This trend highlights the role of branching topology in promoting adsorption of BHPAM on hydrophobic surface. For a given total number of hydrophobic monomers, the increasing in the number of side chains results in a more spatially distributed array of adsorption sites along the polymer backbone. Such widespread distribution of contact points facilitates the formation of multi-point anchoring loop conformation near the surface, thereby alleviating the entropic penalty that typically drives chain desorption. Subsequently, the stability and compactness of the adsorbed layers are enhanced. These observations demonstrate the physical reliability and predictive capability of Atif-V2.0 in analyzing polymer interfacial behavior. This theoretical framework qualitatively captures the impact of polymer topology on adsorption properties, offering valuable insights into the structure–property relationships in polymer flooding. In this work, the many-body topological constraints of polymer chains were incorporated only in the ideal free energy term as shown in ESI. In fact, many-body segment correlations can be introduced *via* second-order thermodynamic perturbation theory (TPT2), which provides a theoretical basis for more accurate descriptions of chain topological effects. We have recently developed a density functional framework named DFT-eTPT2,[60] in which the excess free energy associated with non-bonded chain connectivity is approximated using a combination of TPT1 and TPT2. This framework is expected to complement this current approach in future studies.

Case II: Polymer/Octane/Water Ternary Mixtures

During the actual development of oil reservoirs, the wettability of rock surfaces plays a crucial role in determining oil recovery efficiency. In carbonate reservoirs, the surface typically exhibits

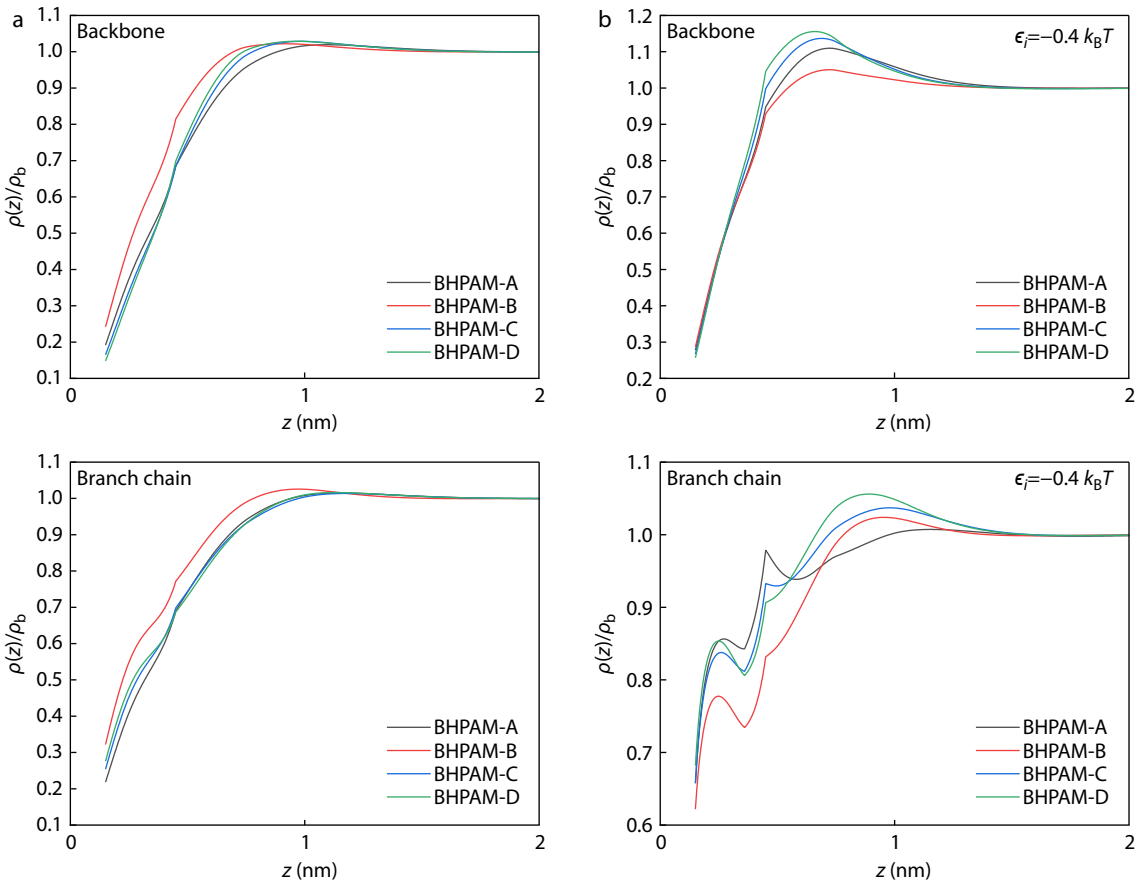

Fig. 3 Normalized density profiles of BHPAM backbone (top) and side chain (bottom) at different interaction strengths. (a) No interaction; (b) ϵ_i = -0.4 k_BT. Black, red, blue, and green curves correspond to BHPAM-A, -B, -C, and -D, respectively.

https://doi.org/10.1007/s10118-025-3412-9

natural oil-wet characteristics.[56] In aged reservoirs that have undergone long-term production and been exposed to asphaltene-rich crude oil, a stable oil film tends to form on the surface.[61] This oil film not only hinders the wetting of the rock surface by the aqueous phase but also suppresses the subsequent infiltration and action of injected polymer solutions. Consequently, in order to get a deeper understanding of the potential performance in displacing oil, it is imperative to develop a rational model to study the thermodynamic behavior of water-soluble polymers near the surfaces covered with oil film.

Hydrophobic groups are often introduced in water-soluble polymers to enhance the interaction between polymers and hydrophobic oil films, which can improve the polymer's ability to strip and displace surface-adsorbed oil. Currently, there are two main strategies for incorporating hydrophobic groups into polymer chains:[62] (1) direct copolymerization of hydrophobic and hydrophilic monomers to form linear copolymers and (2) post-modification of polymer backbones such as grafting hydrophobic side chains. In our previous work, Atif has demonstrated strong analytical capabilities in predicting surficial and interfacial properties of linear polymers.[38,39] In the iSAFT-DFT framework of Atif-V2.0, we extends polymer architecture from linear to branched topologies. In this case, we focus on how grafted hydrophobic side chains influence the thermodynamic properties of polymer/oil/water ternary mixtures. As shown in the inset of Fig. 4(a), two types of polymer structures are selected: HPAM (a linear hydrophilic polymer) and BHPAM (a polymer with hydrophobic side chains grafted onto the hydrophilic backbone). To eliminate the interference of polymer concentration on adsorption behavior, all systems are set to have equal total monomer concentrations, ensuring that the observed effects are due to polymer topology alone. In addition, our model accounts for attractive interactions between octane and surface to mimic the surface environment with residual oil film after water flooding. These interactions are represented by LJ-93 wall potential, analogous to the hydrophobic side chains of polymer.

Experimental and simulation studies have shown that hydrophobically modified polymers can promote a wettability transition from oil-wet to water-wet and improves the displace ability of residual oil.[63,64] This phenomenon is also observed in the calculation results from Atif-V2.0. As shown in Fig. 4, BHPAM exhibits superior water wettability and oil displacement capacity compared to HPAM, as evidenced by a lower density peak of octane and a higher density peak of water. In addition, under the same conditions of attraction strength between the surface and hydrophobic species, the

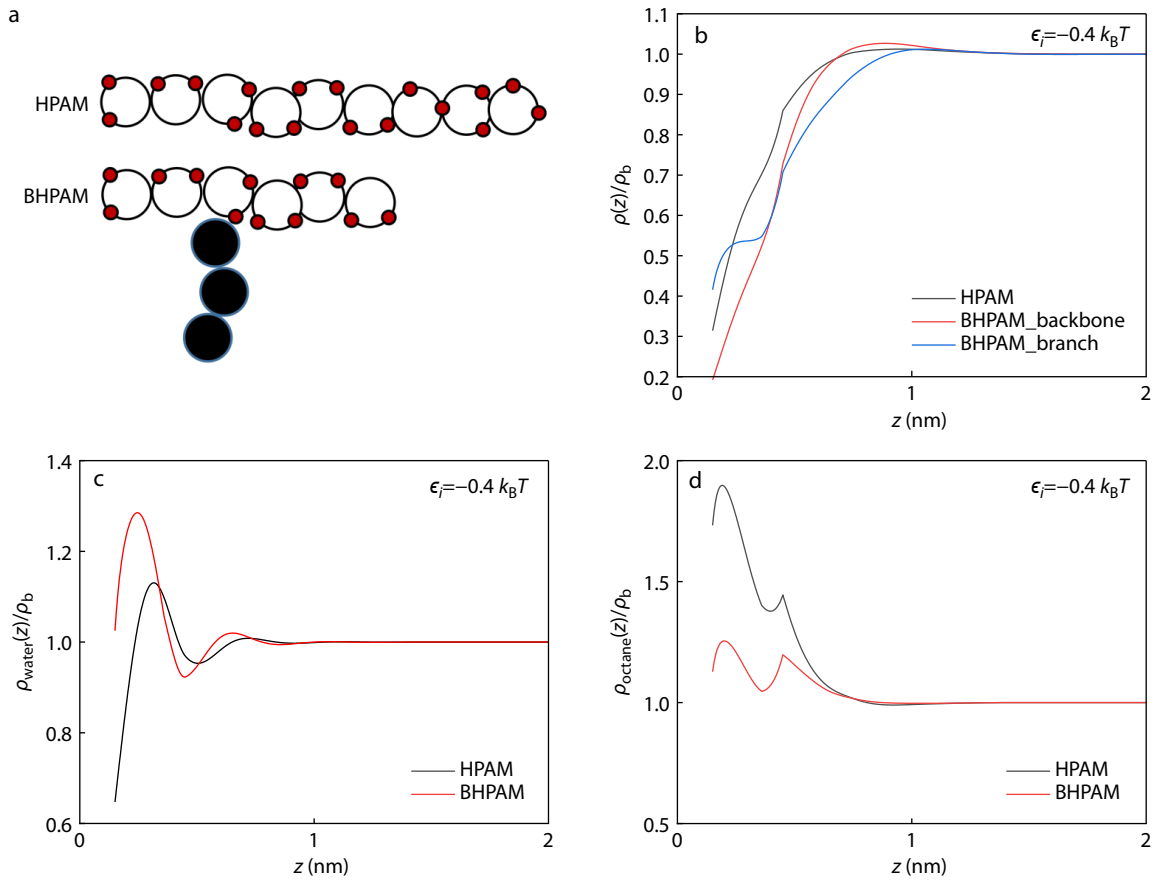

Fig. 4 (a) Schematic diagram illustrating the structure of linear HPAM and hydrophobic-modified BHPAM chain. (b) Normalized density profiles of polymer in polymer/octane/water ternary mixtures. Black, red, and blue curves correspond to linear HPAM chain, the backbone of BHPAM chain, and the branch of BHPAM chain, respectively. Normalized density profiles of (c) water and (d) octane in polymer/octane/water ternary mixtures. Black and red curves correspond to the systems with linear HPAM and BHPAM, respectively. The attraction strength is set to $\epsilon_i = -0.4k_BT$.

https://doi.org/10.1007/s10118-025-3412-9

presence of oil film significantly suppresses polymer adsorption. In both systems with HPAM and BHPAM, the density profiles of polymer are notably reduced compared to the polymer aqueous solution in case I (see Fig. 3b). Nevertheless, the hydrophobic side chains of BHPAM exhibit higher density distribution at the solid–liquid interface than HPAM. This structural feature may be the key factor for its better performance in water wettability and enhancing oil displacement. The above phenomenon that the hydrophobic modification of the polymer enhances the oil displacement ability is also observed when the surface attraction strength is $-0.2k_BT$ (see Fig. S3 in ESI). These findings confirm the critical role of polymer architecture in determining the solid-liquid interfacial behavior of polymer/octane/water mixtures at the molecular level, and further highlight the potential of Atif-V2.0 for studying such solid-liquid phenomena in polymer flooding.

CONCLUSIONS

In this work, we have developed Atif-V2.0 (an advanced theoretical tool for inhomogeneous fluids, Version 2.0), an extended classical density functional theory (cDFT) framework that incorporates polymer topology and hydrogen bonding interactions to model complex multicomponent associating fluids under nanoconfinement. By integrating the interfacial statistical associating fluid theory (iSAFT) approach within the original theoretical framework of Atif, the new version enables the investigation of water-soluble polymers with branched architectures in the presence of alkanes and water, which are representative components of polymer flooding enhanced oil recovery (EOR). Through two case studies, we have demonstrated the predictive power and applicability of Atif-V2.0. In Case I, we investigated the influence of polymer branching topology on the retention behavior of water-soluble polymers in confined porous media. In Case II, we extended this analysis to polymer/oil/water ternary mixtures, revealing the effect of hydrophobic modification on surface wettability and residual oil displacement. Together, these results confirm that Atif-V2.0 provides a versatile molecular-level modeling tool for studying structure–property relationships in confined polymer systems, with direct relevance to EOR polymer design.

Although Atif-V2.0 has demonstrated strong modeling capabilities in polymer/oil/water ternary mixtures, the current implementation does not simultaneously incorporate both explicit hydrogen bonding between water and polymers and electrostatic interactions, which does not attribute to a lack of theoretical foundation. In fact, the original theoretical frame work of Atif already includes an advanced treatment of electrostatics interactions. However, the addition of associative free energy terms in Atif-V2.0 significantly increases the model complexity. Calculating electrostatic interactions under these conditions may lead to numerical convergence issues. Therefore, developing a stable and efficient approach to concurrently address both associative and electrostatics interactions remains a critical challenge for the future enhancements to Atif-V2.0. In addition, it should be noted that the current theoretical framework is built upon Wertheim's first-order thermodynamic perturbation theory, where hydrogen bonding is modeled as localized and orientation-dependent association between discrete sites. While this approach can only partially capture the essential thermodynamics of hydrogen bonding at the molecular level, it does not fully incorporate the formation of extended hydrogen-bonded networks explicitly. Moreover, we have focused on branched topologies in this work, it's worth emphasizing that a more systematic investigation of diverse polymer architectures such as comb-like, star-shaped, and dendritic structures is essential for enabling predictive design of next-generation EOR polymers.

Conflict of Interests

The authors declare no interest conflict.

Electronic Supplementary Information

Electronic supplementary information (ESI) is available free of charge in the online version of this article at http://doi.org/10.1007/s10118-025-3412-9.

Data Availability Statement

The data supporting the findings of this study are available from the corresponding author upon reasonable request. Contact information: cqiuhui@iccas.ac.cn; jiangj@iccas.ac.cn.

ACKNOWLEDGMENTS

This work was financially supported by the Key Technologies R&D Program of China National Offshore Oil Corporation (No. KJGG2021- 0504).

REFERENCES

1 Abdurrahman, M. D.; Pang, A. L.; Arsad, A.; Junin, R.; Syariefudin, M. I.; Regina, S.; Husna, U. Z.; Ahmadipour, M. A short review of biopolymers for enhanced of oil recovery in mature fields. *Pet. Chem.* **2022**, *62*, 482–498.
2 Afolabi, F.; Mahmood, S. M.; Yekeen, N.; Akbari, S.; Sharifigaliuk, H. Polymeric surfactants for enhanced oil recovery: A review of recent progress. *J. Petrol. Sci. Eng.* **2022**, *208*, 109358.
3 Gbadamosi, A. O.; Junin, R.; Manan, M. A.; Yekeen, N.; Augustine, A. Hybrid suspension of polymer and nanoparticles for enhanced oil recovery. *Polym. Bull.* **2019**, *76*, 6193–6230.
4 Mahajan, S.; Yadav, H.; Rellegadla, S.; Agrawal, A. Polymers for enhanced oil recovery: fundamentals and selection criteria revisited. *Appl. Microbiol. Biot.* **2021**, *105*, 8073–8090.
5 Mohsenatabar Firozjaii, A.; Saghafi, H. R. Review on chemical enhanced oil recovery using polymer flooding: Fundamentals, experimental and numerical simulation. *Petroleum* **2020**, *6*, 115–122.
6 Abidin, A.; Puspasari, T.; Nugroho, W. Polymers for enhanced oil recovery technology. *Procedia Chem.* **2012**, *4*, 11–16.
7 Wever, D.; Picchioni, F.; Broekhuis, A. Polymers for enhanced oil recovery: A paradigm for structure–property relationship in aqueous solution. *Prog. Polym. Sci.* **2011**, *36*, 1558–1628.
8 Taylor, K. C.; Nasr-El-Din, H. A. Water-soluble hydrophobically associating polymers for improved oil recovery: A literature review. *J. Petrol. Sci. Eng.* **1998**, *19*, 265–280.

9 Jin, F.-Y.; Li, Q.-H.; He, Y.; Luo, Q.; Pu, W.-F. Experimental study on enhanced oil recovery method in Tahe high-temperature and high-salinity channel sand reservoir: combination of profile control and chemical flooding. *ACS Omega* **2020**, *5*, 5657–5665.
10 Raffa, P.; Picchioni, F. Preliminary evaluation of amphiphilic block polyelectrolytes as potential flooding agents for low salinity chemical enhanced oil recovery. *J. Petrol. Sci. Eng.* **2021**, *198*, 108181.
11 Wu, Q.; Gou, S.; Huang, J.; Fan, G.; Li, S.; Liu, M. Hyper-branched structure—an active carrier for copolymer with surface activity, anti-polyelectrolyte effect and hydrophobic association in enhanced oil recovery. *RSC Adv.* **2019**, *9*, 16406–16417.
12 Afolabi, R. O.; Oluyemi, G. F.; Officer, S.; Ugwu, J. O. Hydrophobically associating polymers for enhanced oil recovery – Part A: A review on the effects of some key reservoir conditions. *J. Petrol. Sci. Eng.* **2019**, *180*, 681–698.
13 de Vasconcelos, C. K. B.; Lopes, R. C. F. G.; Medeiros, F. S.; Viana, M. M.; Caliman, V.; Silva, G. G. Rheological and structural properties of nanofluids based on hydrolyzed polyacrylamide and aminated carbon nanotubes for enhanced oil recovery. *Polymer* **2024**, *307*, 127325.
14 Patel, V.; Dalsania, Y.; Azad, M. S.; Sharma, T.; Trivedi, J. Characterization of co- and post-hydrolyzed polyacrylamide molecular weight and radius distribution under saline environment. *J. Appl. Polym. Sci.* **2021**, *138*, 50616.
15 Chen, P.; Yao, L.; Liu, Y.; Luo, J.; Zhou, G.; Jiang, B. Experimental and theoretical study of dilute polyacrylamide solutions: effect of salt concentration. *J. Mol. Model.* **2012**, *18*, 3153–3160.
16 Yang, S.; Ma, T.; He, Y.; Su, X. The molecular explanation for polyacrylamide viscosity reduction in high-salinity formation-water. *AIP Adv.* **2021**, *11*, 1–10.
17 Aguirre Giraldo, A.; Moncayo-Riascos, I.; Ribadeneira, R. Effect of the Cations (Na+, Ca2+, Fe2+, and Fe3+) on the Partially hydrolyzed polyacrylamide shrinking by molecular dynamics simulations. *Energ. Fuel.* **2022**, *36*, 5228–5239.
18 Zhang, K.; Choi, H. J.; Jang, C. H. Turbulent drag reduction characteristics of poly(acrylamide-co-acrylic acid) in a rotating disk apparatus. *Colloid Polym. Sci.* **2011**, *289*, 1821–1827.
19 Oliveira, P. F.; Costa, J. A.; Oliveira, L. F. S.; Mota, L. S.; de Oliveira, L. A.; Mansur, C. R. E. Hydrolysis and thermal stability of partially hydrolyzed polyacrylamide in high-salinity environments. *J. Appl. Polym. Sci.* **2019**, *136*, 47793.
20 Yuan, S.; Guo, A.; Zhang, H.; Wang, Z.; Yuan, S. Molecular dynamics simulations of supramolecular polymers within nanoconfinements for enhanced oil recovery. *ACS Appl. Mater. Interfaces* **2024**, *16*, 5255–5267.
21 Yao, L.; Chen, P.; Ding, B.; Luo, J.; Jiang, B.; Zhou, G. Molecular design of modified polyacrylamide for the salt tolerance. *J. Mol. Model.* **2012**, *18*, 4529–4545.
22 Nair, N.; Park, M.; Handgraaf, J. W.; Cassiola, F. M. Coarse-grained simulations of polymer-grafted nanoparticles: structural stability and interfacial Behavior. *J. Phys. Chem. B* **2016**, *120*, 9523–9539.
23 Fu, L.; Gu, F.; Liao, K.; Wen, X.; Huang, W.; Li, X.; Ren, Z.; Xie, L. Application of molecular simulation in tertiary oil recovery: a systematic review. *J. Petrol. Sci. Eng.* **2022**, *212*, 110196.
24 Liu, Z.; Feng, Q.; Xu, Z.; Yang, S. Research progress of molecular simulation in acrylamide polymers with high degree of polymerization. *Molecules* **2024**, *29*, 2589.
25 Wever, D. A. Z.; Picchioni, F.; Broekhuis, A. A. Comb-like polyacrylamides as flooding agent in enhanced oil recovery. *Ind. Eng. Chem. Res.* **2013**, *52*, 16352–16363.
26 Pu, W. F.; Liu, R.; Wang, K. Y.; Li, K. X.; Yan, Z. P.; Li, B.; Zhao, L. Water-soluble core-shell hyperbranched polymers for enhanced oil recovery. *Ind. Eng. Chem. Res.* **2015**, *54*, 798–807.
27 Du, D. J.; Pu, W. F.; Tang, Z. J.; Liu, R.; Han, S. H.; Zhang, W. H.; Zhao, B.; Wei, J. Solution properties and displacement characteristics of core-shell hyperbranched associative polyacrylamide for enhanced oil recovery. *Energ. Fuel.* **2018**, *32*, 8154–8166.
28 Klemm, B.; Picchioni, F.; Raffa, P.; van Mastrigt, F. Star-like branched polyacrylamides by RAFT polymerization, part II: performance evaluation in enhanced oil recovery (EOR). *Ind. Eng. Chem. Res.* **2018**, *57*, 8835–8844.
29 Shi, L. T.; Li, C.; Zhu, S. S.; Xu, J.; Sun, B. Z.; Ye, Z. B. Study on properties of branched hydrophobically modified polyacrylamide for polymer flooding. *J. Chem.* **2013**, *2013*, 675826.
30 Unke, O. T.; Chmiela, S.; Sauceda, H. E.; Gastegger, M.; Poltavsky, I.; Schütt, K. T.; Tkatchenko, A.; Müller, K. R. Machine learning force fields. *Chem. Rev.* **2021**, *121*, 10142–10186.
31 Hu, J.; Zhou, L.; Jiang, J. Efficient machine learning force field for large-scale molecular simulations of organic systems. *CCS Chem.* **2025**, *7*, 716–730.
32 Wu, J. Density functional theory for chemical engineering: From capillarity to soft materials. *AIChE J.* **2006**, *52*, 1169–1193.
33 Tarazona, P.; and, R. E. A simple density functional theory for inhomogeneous liquids. *Mol. Phys.* **1984**, *52*, 847–857.
34 Tarazona, P. Free-energy density functional for hard spheres. Phys. Rev. A 1985, 31, 2672–2679.
35 Yu, Y.-X.; Wu, J. Density functional theory for inhomogeneous mixtures of polymeric fluids. *J. Chem. Phys.* **2002**, *117*, 2368–2376.
36 Jiang, J.; Ginzburg, V. V.; Wang, Z.-G. Density functional theory for charged fluids. *Soft Matter* **2018**, *14*, 5878–5887.
37 Jiang, J. Software package: an advanced theoretical tool for inhomogeneous fluids (Atif). *Chinese J. Polym. Sci.* **2022**, *40*, 220–230.
38 Chang, Q.; Jiang, J. Force regulation by sequence-defined polyelectrolytes. *Macromolecules* **2023**, *56*, 4100–4110.
39 Chang, Q.; Jiang, J. Nanoscale hierarchical structures formed by sequence-defined polycations and homopolyanions for high salt-tolerance adhesives. *Macromolecules* **2024**, *57*, 1859–1867.
40 Chang, Q.; Wang, R.; Qing, L.; Jiang, J. Trends in sequence-defined polyelectrolyte systems: a perspective. *Chinese J. Polym. Sci.* **2025**, *43*, 1–17.
41 Jackson, G.; Chapman, W. G.; and, K. E. G. Phase equilibria of associating fluids: spherical molecules with multiple bonding sites. *Mol. Phys.* **1988**, *65*, 1–31.
42 Chapman, W. G.; Jackson, G.; and, K. E. G. Phase equilibria of associating fluids: chain molecules with multiple bonding sites. *Mol. Phys.* **1988**, *65*, 1057–1079.
43 Chapman, W.; Gubbins, K.; Jackson, G.; Radosz, M. SAFT: equation-of-state solution model for associating fluids. *Fluid Phase Equilibr.* **1989**, *52*, 31–38.
44 Gross, J.; Sadowski, G. Perturbed-chain SAFT: an equation of state based on a perturbation theory for chain molecules. *Ind. Eng. Chem. Res.* **2001**, *40*, 1244–1260.
45 Gil-Villegas, A.; Galindo, A.; Whitehead, P. J.; Mills, S. J.; Jackson, G.; Burgess, A. N. Statistical associating fluid theory for chain molecules with attractive potentials of variable range. *J. Chem. Phys.* **1997**, *106*, 4168–4186
46 Wang, L.; Haghmoradi, A.; Liu, J.; Xi, S.; Hirasaki, G. J.; Miller, C. A.; Chapman, W. G. Modeling micelle formation and interfacial properties with iSAFT classical density functional theory. *J. Chem. Phys.* **2017**, *146*, 124705.
47 Tripathi, S.; Chapman, W. G. Microstructure of inhomogeneous polyatomic mixtures from a density functional formalism for atomic mixtures. *J. Chem. Phys.* **2005**, *122*, 094506.
48 Lymperiadis, A.; Adjiman, C. S.; Galindo, A.; Jackson, G. A group contribution method for associating chain molecules based on

the statistical associating fluid theory (SAFT- γ). *J. Chem. Phys.* **2007**, *127*, 234903.
49 de Freitas Gonçalves, A.; Amancio, R. J.; Castier, M.; Franco, L. F. M. Classical density functional theory consistent with the SAFT-VR Mie equation of state: development of functionals and application to confined fluids. *J. Chem. Eng. Data* **2024**, *69*, 3645–3659.
50 Malheiro, C.; Mendiboure, B.; Plantier, F.; Blas, F. J.; Miqueu, C. Density functional theory for the description of spherical non-associating monomers in confined media using the SAFT-VR equation of state and weighted density approximations. *J. Chem. Phys.* **2014**, *140*, 134707.
51 Sauer, E.; Gross, J. Classical density functional theory for liquid–fluid interfaces and confined systems: a functional for the perturbed-chain polar statistical associating fluid theory equation of state. *Ind. Eng. Chem. Res.* **2017**, *56*, 4119–4135.
52 Tripathi, S.; Chapman, W. G. Microstructure and thermodynamics of inhomogeneous polymer blends and solutions. *Phys. Rev. Lett.* **2005**, *94*, 087801.
53 Eller, J.; Matzerath, T.; van Westen, T.; Gross, J. Predicting solvation free energies in non-polar solvents using classical density functional theory based on the PC-SAFT equation of state. *J. Chem. Phys.* **2021**, *154*, 244106.
54 Yu, Y. X.; Wu, J. A fundamental-measure theory for inhomogeneous associating fluids. *J. Chem. Phys.* **2002**, *116*, 7094–7103.
55 Rosenfeld, Y. Free-energy model for the inhomogeneous hard-sphere fluid mixture and density-functional theory of freezing. *Phys. Rev. Lett.* **1989**, *63*, 980–983.
56 Ekanem, E. M.; Rücker, M.; Yesufu-Rufai, S.; Spurin, C.; Ooi, N.; Georgiadis, A.; Berg, S.; Luckham, P. F. Novel adsorption mechanisms identified for polymer retention in carbonate rocks. *JCIS Open* **2021**, *4*, 100026.
57 Gbadamosi, A.; Patil, S.; Kamal, M. S.; Adewunmi, A. A.; Yusuff, A. S.; Agi, A.; Oseh, J. Application of polymers for chemical enhanced oil recovery: a review. *Polymers* **2022**, *14*, 1433.
58 Källrot, N.; Dahlqvist, M.; Linse, P. Dynamics of polymer adsorption from bulk solution onto planar surfaces. *Macromolecules* **2009**, *42*, 3641–3649.
59 Semenov, A. N.; Bonet-Avalos, J.; Johner, A.; Joanny, J. F. Adsorption of polymer solutions onto a flat surface. *Macromolecules* **1996**, *29*, 2179–2196.
60 Qing, L.; Wang, X.; Li, S.; Zhang, J.; Jiang, J. Thermodynamic perturbation theory for charged branched polymers. *J. Chem. Theory Comput.* **2025**, *21*, 333–346.
61 Buckley, J. S.; Liu, Y.; Monsterleet, S. Mechanisms of wetting alteration by crude oils. *SPE Journal* **1998**, *3*, 54–61.
62 Feng, Y.; Billon, L.; Grassl, B.; Khoukh, A.; François, J. Hydrophobically associating polyacrylamides and their partially hydrolyzed derivatives prepared by post-modification. 1. Synthesis and characterization. *Polymer* **2002**, *43*, 2055–2064.
63 Zou, W.; Fang, Z.; Zhang, Z.; Lu, Z. Interaction and adsorption of hydrophobically modified polyacrylamide on silica and asphaltene surfaces. *Adv. Polym. Technol.* **2019**, *2019*, 5423178.
64 Ahsani, T.; Tamsilian, Y.; Rezaei, A. Molecular dynamic simulation and experimental study of wettability alteration by hydrolyzed polyacrylamide for enhanced oil recovery: A new finding for polymer flooding process. *J. Petrol. Sci. Eng.* **2021**, *196*, 108029.

https://doi.org/10.1007/s10118-025-3412-9